AIAA JOURNAL
Vol. 31, No. 9, September 1993

Evaluation of Algebraic Eddy-Viscosity Models in Three-Dimensional Turbulent Boundary-Layer Flows

M. Semih Ölçmen and Roger L. Simpson
Virginia Polytechnic Institute and State University, Blacksburg, Virginia 24060

Nomenclature

A_1 = Townsend's structural parameter, $\frac{\sqrt{\overline{uv}^2 + \overline{vw}^2}}{\overline{u^2} + \overline{v^2} + \overline{w^2}}$
D = diameter of circular cylinder
N = anisotropy constant, $\frac{-\overline{vw}/(\partial W/\partial y)}{-\overline{uv}/(\partial U/\partial y)}$
U_{ref} = reference velocity
$\overline{u^2}, \overline{v^2}, \overline{w^2}$ = kinematic normal stresses
$-\overline{uv}, -\overline{uw}, -\overline{vw}$ = kinematic shear stresses
W_0 = surface velocity of rotating cylinder
α = flow angle with respect to x_{FS} axis of local freestream coordinates
α_g = mean velocity gradient vector angle with respect to the x_{FS} axis of the local freestream coordinates
α_m = measured shear stress vector angle with respect to the x_{FS} axis of the local freestream coordinates
ν = kinematic viscosity

I. Introduction

THE exact three-dimensional, unsteady Navier-Stokes equations cannot be solved yet due mainly to the limited capacity and speed of present computers, which are necessary in taking into account the fine scales of the flows. Since the Reynolds-averaged equations have more unknowns than the number of equations, the approach to overcome the difficulty has been to develop new equations for the unknowns in terms of the other unknowns so that the problem can be mathematically closed. The currently used models for turbulence closure were reviewed by several authors.[1-8]

The purpose of this work is to evaluate the relative performance of some turbulence models directly from experimental data rather than calculations. In this study selected models that did not necessitate solving the momentum, continuity, and turbulent transport equations were chosen so that the necessary mean velocity and gradient terms, shear stress magnitude at the wall, and maximum shear stress location and magnitude in the profiles could be supplied directly from the measured data. All the quantities leading to the calculation of eddy viscosities and shear stresses with the models were calculated using only the data. This restricts the discussion to algebraic eddy-viscosity models.

The idea behind the algebraic eddy-viscosity models is that the turbulent shear stresses could be related to the mean flow quantities in a similar fashion as in laminar or molecular stresses. Since the eddy viscosity is not a property of the fluid but of the flow and also changes from point to point in the flow, it was seen as not suitable for the closure of turbulence.[9] However, most of the available computational schemes tend to use this type of model[3] due to its programming simplicity and speed, but the results are inadequate or are only in qualitative agreement with Reynolds shear stress data.[10-20] The eddy viscosity was further developed by several researchers to take into account the differences between the measured and predicted shear stresses. The anisotropic eddy viscosity of Rotta,[21] Rhyming and Fannelop,[22] and Humphreys[23] were seen to calculate some flows rather well and some rather poorly.[23-25]

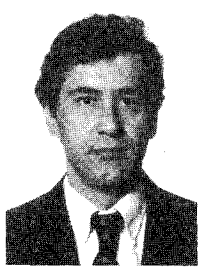

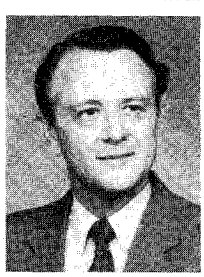

Dr. M. S. Ölçmen received a B.S. degree in Aeronautical Engineering from İstanbul Technical University in 1982, and a post-graduate degree from the Von Kármán Institute in Belgium in 1983. He received an M.S. degree in Aeronautical Engineering in 1985 from İstanbul Technical University partly under a Turkish Scientific and Technical Research Association award. After being granted a scholarship by the Ministry of National Education, Youth and Sports of Turkey, he received a Ph.D. degree from the Aerospace and Ocean Engineering Department at Virginia Polytechnic Institute and State University in 1990. He has worked as a researcher on three-dimensional turbulent flows sponsored by the Advanced Research Project Agency and the Office of Naval Research. At present he is a Research Associate at the Aerospace and Ocean Engineering Department at Virginia Polytechnic Institute and State University and is a member of AIAA.

Dr. Roger L. Simpson received his B.S. in Mechanical Engineering from the University of Virginia and M.S. and Ph.D. degrees in Mechanical Engineering from Stanford University. Since 1965 he has been involved with experimental research on the structure and control of the Department of Defense and NASA. He has developed special two-phase flow and unsteady flow wind tunnel facilities and equipment, frequency-domain laser-Doppler anemometer signal processing for early 1970s separated flow research, advanced LDA and surface-pressure fluctuation signal processing techniques, and other state-of-the-art instrumentation. From 1969 to 1983 he was Professor at Cowling Professorship in the Department of Aerospace and Ocean Engineering at Virginia Tech and is now the Director of the Stability Wind Tunnel. Dr. Simpson is a Fellow of the AIAA, the ASME, and the Institute of Diagnostic Engineers (U.K.). He is a former associate editor of the *AIAA Journal*, a former member of the AIAA Fluid Dynamics Technical Committee, and has organized several AIAA meetings. Currently he is serving on the AIAA Board of Directors.

Received Aug. 15, 1992; revision received Feb. 3, 1993; accepted for publication Feb. 4, 1993.

In the following sections, the experimental data and the selected turbulence models will be summarized. The shear stress direction and magnitude as calculated by the models will be discussed. Conclusions about the relative performance of these models will be made.

II. Experimental Data

The validity of the turbulence models for three-dimensional turbulent boundary layers (TBLs) was tested within the limits of the available data. As pointed out by Bradshaw,[26] the study of the effect of the three dimensionality of the flow on the turbulence structure still necessitates further reliable data sets that include all terms of the Reynolds stress tensor. Previous reviews of the available three-dimensional TBL data were made by several authors, including Fernholz and Vagt,[27] Anderson and Eaton,[28] and Van Den Berg.[29] In this study the data sets that included all of the Reynolds stresses and wall skin friction magnitude and direction were chosen.

The pressure-driven experimental data chosen were of Anderson and Eaton,[28,30] Dechow and Felsch,[31] Dechow,[32] Müller,[33] Elsenaar and Boelsma,[34] and Ölçmen.[35] The shear-driven data were taken from Bissonnette and Mellor[36] and Lohmann.[37] For the pressure-driven flows, the local freestream flow has the curvature of one sign, with exception of the Ölçmen flow. For the Ölçmen flow, the last two stations have a local freestream curvature of the opposite sign from the upstream stations. A summary of the flow conditions, the techniques used to measure the stress and mean velocity in the flow and the skin friction at the wall, and some of the important conclusions obtained from those studies may be found in Table 1. All of the data sets used were first expressed in local freestream coordinates (x_{FS} is parallel to the wall and in the direction of the streamwise velocity vector at the boundary layer edge; y_{FS} is perpendicular to the wall; and z_{FS} completes a right-handed coordinate system).

III. Selected Algebraic Turbulence Models

The turbulence models selected were chosen from among the models that did not necessitate solving the governing

Table 1 Summary of experimental data sets

Authors	Flow studied	Measurement method for mean velocity and Reynolds shear stress tensor	Method for skin-friction measurements	U_{ref}/ν of the flow and station numbers used	Some important conclusions of the study
Anderson-Eaton	Flow towards a 90-deg wedge	X wire, 3,4 hole probe	Surface fence	$U_{ref}/\nu = 1.023 \times 10^6$/m S1, S2, S3, S4, S5	N changes -1.0 to 0.5; A_1 is not a constant, changes from ≈ 0.14 to ≈ 0.04 proceeding downstream; α_m lags α_g
Müller	Three-dimensional flow created by transverse and lateral pressure gradients with use of turning vanes on a flat plate	X wire	Preston tubes	$U_{ref}/\nu = 1.95 \times 10^6$/m A1, B1, C2, D2, E3, F5	N above $y^+ = 100$ scattered around ≈ 1.5; A_1 is scattered around ≈ 0.14; α_m leads α_g at some stations, velocity skewed down to the wall
Dechow-Felsch	Three-dimensional flow induced by a cylinder standing on a flat plate	Conrad tube, boundary-layer-type single wire, X wire	Preston tube	$U_{ref}/\nu = 1.451 \times 10^6$/m 1, 2, 3, 4, 5, 6, 7	Flow is anisotropic, N changes from ≈ -2 to ≈ 0.5; A_1 is not a constant, changes from ≈ 0.14 to ≈ 0.06 proceeding downstream; α_m lags α_g
Elsenaar-Boelsma	Incompressible turbulent boundary layer under infinite swept conditions in an adverse pressure gradient	X wire, slanted wire, single straight wire, cobra probe	Stanton type surface pressure probes, Clauser plots	$U_{ref}/\nu = 2.42 \times 10^6$/m 1, 4, 5, 6, 7, 8, 9, 10	N changes from ≈ -0.5 to 0.75; A_1 is not a constant, changes from ≈ 0.15 to ≈ 0.08 proceeding downstream, below $y^+ = 1000$; flow is anisotropic; α_m lags σ_g.
Ölçmen	Three-dimensional flow induced by 3:2 elliptical nosed NACA 0020 tailed body protruding from a flat plate	Laser-Doppler-velocimeter, single hot wire	Skin-friction interferometer	$U_{ref}/\nu = 1.726 \times 10^6$/m 0, 1, 2, 3, 4, 5, 6, 7, 8	N changes from ≈ -0.5 to ≈ 1.0; flow is not isotropic; α_m lags α_g; A_1 is not a constant, changes from ≈ 0.03 to 0.22
Bissonnette-Mellor	Three-dimensional turbulent boundary layer on an axially rotating cylinder	Straight and slanted wires	Obtained by extrapolating the data to the wall	U_{ref}*D/2$\nu = 4.14 \times 10^4$ for low Re, U_{ref}*D/2$\nu = 7.95 \times 10^4$ for high Re data; $D = 5$ in.; W_0 kept constant; 5, 6, 7, 8 for both Re	N changes from ≈ 0.5 to 1.4 for low Re and from ≈ 0.4 to 1.2 for high Re; flow is collateral near the wall in a rotating frame of reference; A_1 is not a constant, varies from ≈ 0.12 to 0.2; α_m lags α_g
Lohmann	Three-dimensional turbulent boundary layer formed on an axially rotating cylinder	Slanted wire, single wire	Obtained from Clauser plots	U_{ref}*D/$\nu = 2.9 \times 10^5$, $D = 10$ in.; $W_0/U_{ref} = 1.65$; 2, 4, 9	N varies from ≈ 0.5 to ≈ 1.7 below $y^+ < 600$; A_1 is not a constant, varies from ≈ 0.12 to ≈ 0.21; near-wall flow was collateral; α_m leads α_g

continuity, momentum, and turbulent transport equations. This choice restricts the discussion to algebraic eddy viscosity models.

The comparison of the computed and experimental data was performed using two parameters, a magnitude ratio and an angle difference, which are described later. The shear stress vector in the plane parallel to the floor with components of $-\overline{vw}_{FS}$ and $-\overline{uv}_{FS}$ can be expressed using complex numbers in the form $|\tau|e^{i\alpha}$, where $|\tau| = [-\overline{uv}_{FS}^2 + (-\overline{vw}_{FS}^2)]^{1/2}$ and α is the shear stress angle with respect to the x axis of the local freestream coordinates. The ratio of the measured and computed shear stresses presented in the complex form give two parameters:

$$\frac{|\tau_m|}{|\tau_c|} = \text{magnitude ratio}$$

$$\alpha_m - \alpha_c = \text{angle difference}$$

where m denotes the measured quantities and c stands for the computed values. If a model were able to calculate the magnitude and the direction of the measured shear stress vector data perfectly, the ratio of magnitudes would be 1, and the difference between the shear stress directions would be 0. In the present paper, for each data set and model, an average of the magnitude ratio ($\overline{\tau_m/\tau_c}$) and an average of the angle difference ($\overline{\alpha_m - \alpha_c}$) and the standard deviation of these quantities from the mean were calculated for a given y^+ ($= yu_\tau/\nu$; $u_\tau = \sqrt{\tau_w/\rho}$; ρ = density; τ_w = skin-friction magnitude at the wall) using

$$\delta_\tau = \left\{\frac{1}{(S-1)}\sum_{i=1}^{S}[(\tau_m/\tau_c)_i - \overline{(\tau_m/\tau_c)}]^2\right\}^{1/2}$$

$$\delta_\alpha = \left\{\frac{1}{(S-1)}\sum_{i=1}^{S}[(\alpha_m - \alpha_c)_i - \overline{(\alpha_m - \alpha_c)}]^2\right\}^{1/2}$$

and are presented in Figs. 1-8. S denotes the total number of samples used in averaging. The averaging was carried out at 25 different y^+ points, which were equally spaced in the logarithmic scale between $y^+ = 10$ and $y^+ = 5000$ among the profiles of a particular data set at these y^+ locations. At the y^+ locations where the magnitude ratio and the angle difference were not available, the quantities were found with a linear interpolation between the quantities at one upper and at one lower y^+ location.

All of the computations were carried out using the data in local freestream coordinates, and U and W denote the mean velocity components in the x_{FS} and z_{FS} directions, respectively. The necessary mean flow gradients to calculate computed shear stresses for each flow were found by fitting a parabola to five consecutive points of the mean velocity profiles and computing the gradients at the third, or middle, point. For Ölçmen's data set the shear stresses at the wall were taken from Ailinger[38] except at the zeroth and first stations. That study was done under the same flow conditions to obtain the wall skin friction magnitude and direction with an oil-flow skin-friction interferometer technique. At station 0, the wall stress was found using the two-dimensional law of the wall Clauser plot. At station 1, Johnston's three-dimensional law of the wall was used.[35]

For all of the other data sets, measured wall stresses were used. For all of the data sets the required mean flow quantities were also taken from the data, as if the solutions of the governing equations were the same as the data. The necessary maximum shear stress magnitudes in the layers for the Johnson-King model for each data set at each station were taken as the measured maximum shear stress magnitudes that satisfied the realizability conditions.[39] These conditions are

$$\text{determinant}(R_{ij}) \geq 0$$

$$R_{ij}^2 \leq R_{ii}R_{jj} \quad \text{for } i \neq j$$

$$R_{ij} \geq 0 \quad \text{for } i = j$$

in which the summation convention is not used (R_{ij} = Reynolds stress tensor). Also in the calculation of the magnitude ratio for all of the data sets the measured stresses that fully satisfied these conditions were used.

A. Cebeci-Smith Model

The Cebeci-Smith (C-S) model used in this study[40] uses two different eddy-viscosity definitions, one described for the inner region and one for the outer region. In the inner region, the eddy-viscosity is defined as

$$\nu_{ti} = F^2 l^2\left[\left(\frac{\partial U}{\partial y}\right)^2 + \left(\frac{\partial W}{\partial y}\right)^2\right]^{1/2}$$

$$l = \kappa y, \qquad F = 1 - \exp(-y^+/A^+)$$

$$A^+ = 26 \qquad \kappa = 0.4$$

where l is the mixing length, F is the Van Driest damping function, and κ is the von Kármán constant.

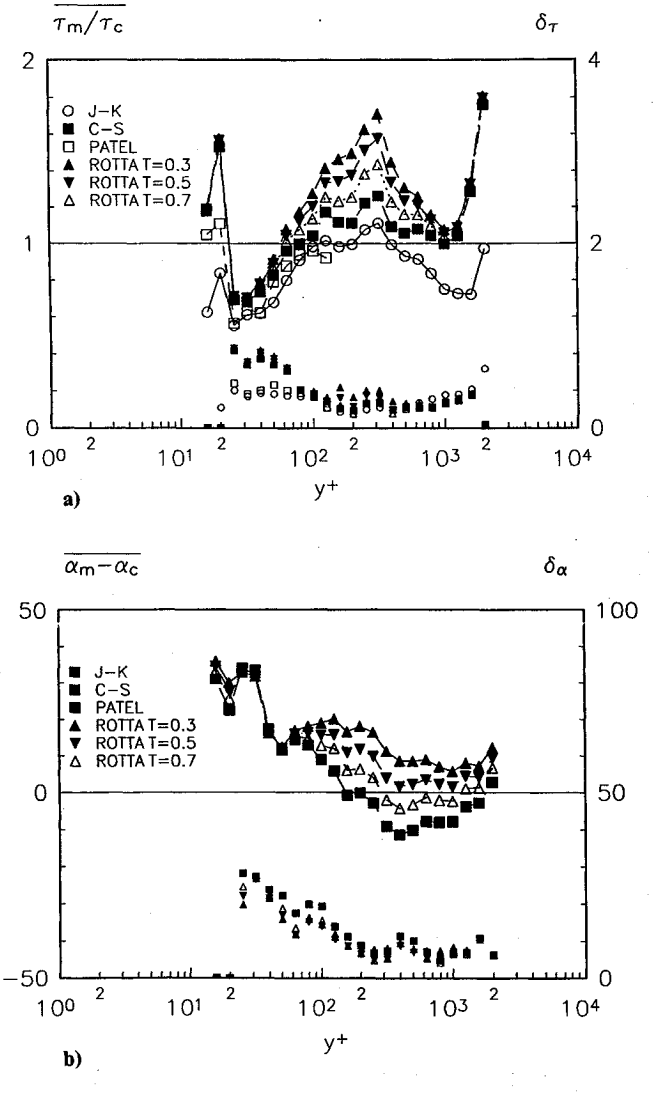

Fig. 1 a) Average magnitude ratio and b) average angle difference and the standard deviations on these quantities around the mean calculated with several models for Ölçmen flow. Right-hand-side ordinate and smaller symbols are used for the standard deviations.

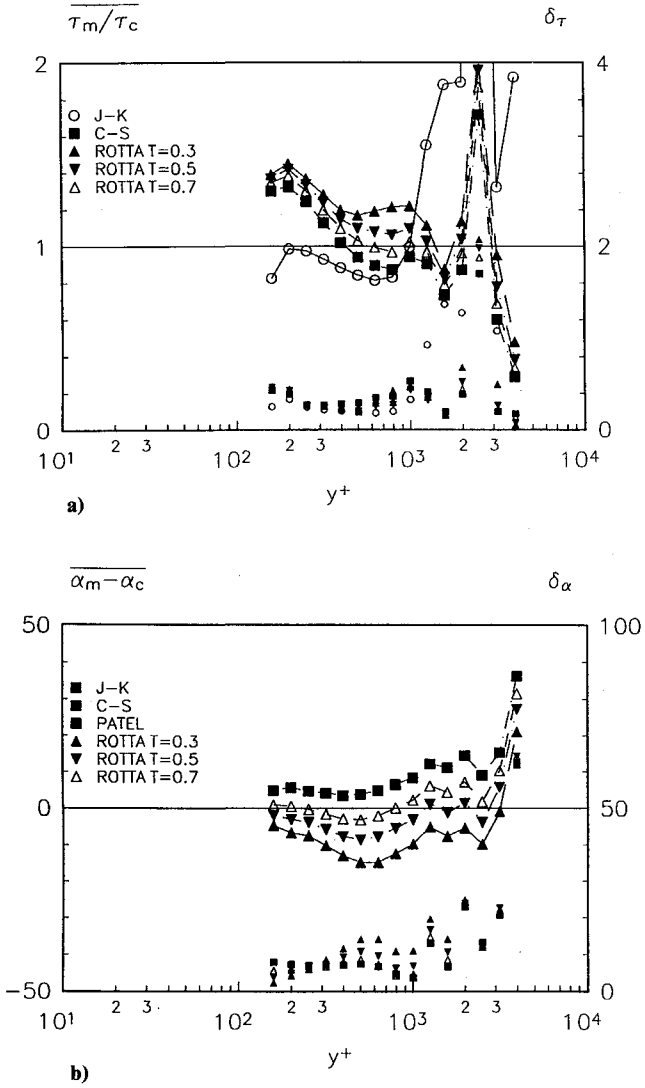

Fig. 2 a) Average magnitude ratio and b) average angle difference and the standard deviations on these quantities around the mean calculated with several models for Elsenaar-Boelsma flow. Right-hand-side ordinate and smaller symbols are used for the standard deviations.

The outer region eddy-viscosity is given by

$$\nu_{to} = 0.0168\,\delta_2^*\gamma_k U_e$$

$$\delta_2^* = \left|\int_0^\infty \left(1 - \frac{(U^2+W^2)^{1/2}}{U_e}\right)dy\right|$$

in which δ_2^* is the displacement thickness, γ_k is Klebanoff's intermittency correction, and U_e is the local freestream velocity outside of the boundary layer at that streamwise location. The boundary-layer thickness δ is defined[3] as the point in the layer where $(U^2+W^2)/U_e^2$ is 0.99.

By using a smoothing function, the eddy-viscosity distribution in the layer can be defined as

$$\nu_t = \nu_{to}[1 - \exp(-\nu_{ti}/\nu_{to})]$$

and the shear stresses are found by using

$$-\overline{uv}_{FS} = \nu_t \frac{\partial U}{\partial y}, \qquad -\overline{vw}_{FS} = \nu_t \frac{\partial W}{\partial y}$$

B. Rotta Model

This anisotropic eddy-viscosity model is based on work by Rotta.[41] An analysis of the pressure strain terms in the governing equations for the stresses led Rotta to an anisotropic eddy-viscosity model.[21] The model uses an anisotropy constant T

$$T = \frac{(\nu_T)_{\text{transverse}}}{(\nu_T)_{\text{streamwise}}}$$

defined as the ratio of the transverse eddy viscosity to the streamwise eddy viscosity in local streamwise coordinates.

By assuming T constant in the layer, ν_T in the local freestream coordinates can be computed as

$$\nu_T = F^2 l^2 \left[\left(\frac{\partial U}{\partial y}\right)^2 + \left(\frac{\partial W}{\partial y}\right)^2 + \frac{(T-1)[W(\partial U/\partial y) - U(\partial W/\partial y)]^2}{U^2+W^2}\right]^{1/2}$$

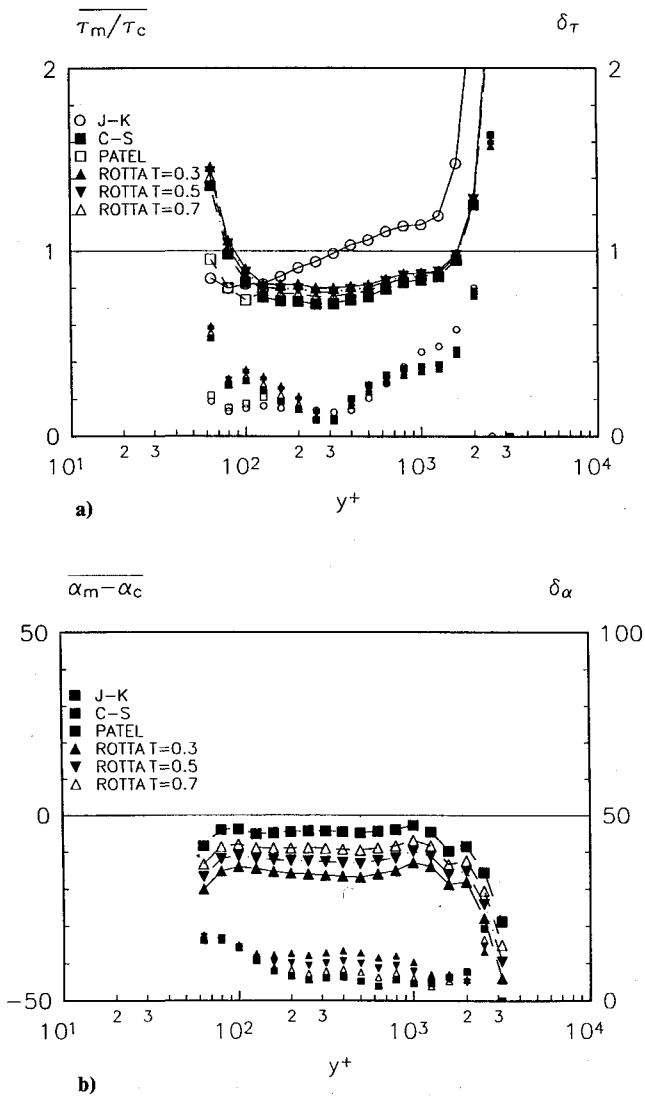

Fig. 3 a) Average magnitude ratio and b) average angle difference and the standard deviations on these quantities around the mean calculated with several models for Müller flow. Right-hand-side ordinate and smaller symbols are used for the standard deviations.

and the stresses are related to the mean flow gradients with

$$\nu_t = \nu_{to}[1 - \exp(-\nu_T/\nu_{to})]$$

$$-\overline{uv}_{FS} = \nu_t\left(a_{xx}\frac{\partial U}{\partial y} + a_{xz}\frac{\partial W}{\partial y}\right)$$

$$-\overline{vw}_{FS} = \nu_t\left(a_{xz}\frac{\partial U}{\partial y} + a_{zz}\frac{\partial W}{\partial y}\right)$$

where

$$a_{xx} = \frac{U^2 + TW^2}{U^2 + W^2} \qquad a_{zz} = \frac{W^2 + TU^2}{U^2 + W^2}$$

$$a_{xz} = (1 - T)\frac{UW}{U^2 + W^2} \qquad l = \kappa y$$

In this study, following Abid,[47] ν_T as defined by Rotta was used as the inner layer eddy viscosity, and the outer layer eddy viscosity ν_{to} was kept the same as the Cebeci-Smith model. The anisotropy constant $T = 1$ corresponds to isotropic turbulence and $T \neq 1$ to anisotropic turbulence. For the present data, five

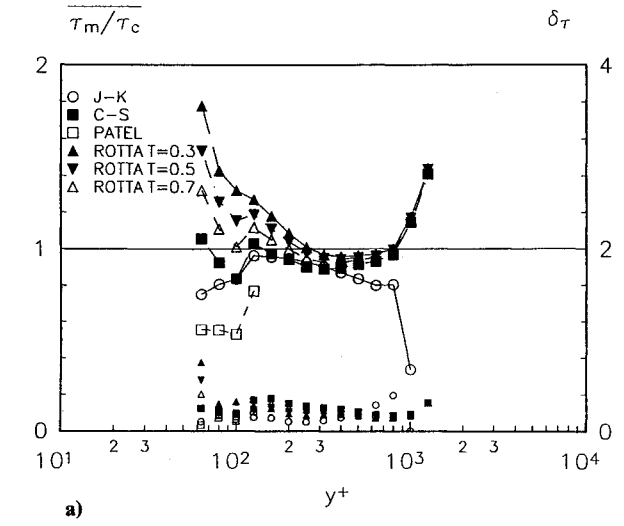

Fig. 4 a) Average magnitude ratio and b) average angle difference and the standard deviations on these quantities around the mean calculated with several models for Dechow-Felsch flow. Right-hand-side ordinate and smaller symbols are used for the standard deviations.

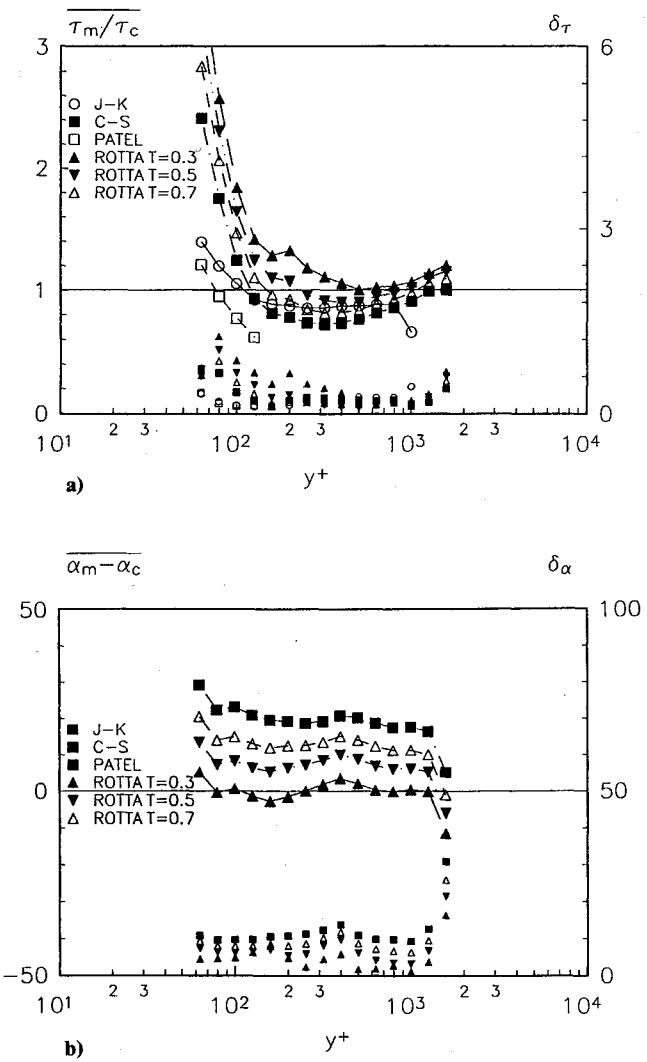

Fig. 5 a) Average magnitude ratio and b) average angle difference and the standard deviations on these quantities around the mean calculated with several models for Anderson flow. Right-hand-side ordinate and smaller symbols are used for the standard deviations.

data, five different anisotropy constants, $T = 0.3$, 0.5, 0.7, 1.2, and 1.5 were tested. Cases with $T > 1$ imply that the effective spanwise eddy viscosity is larger than the streamwise eddy viscosity. In other terms T can be expressed as

$$T = \frac{\tan(\alpha_m - \alpha)}{\tan(\alpha_g - \alpha)}$$

If T is larger than 1, it can be seen that $|\alpha_m - \alpha|$ is larger than $|\alpha_g - \alpha|$, which are the cases for Lohmann and Müller flows. Calculations with $T > 1$ are presented for the shear-driven flows since the agreement with the measurements is better than the calculations made with $T < 1$.

C. Patel's Model

The third model selected is the one equation (k) near-wall model of Wolfshtein[42] as used by Chen and Patel[43] in the k-ϵ turbulence model with the fully elliptic Reynolds-averaged Navier-Stokes equations to compute the flow characteristics in the boundary layer or wake of axisymmetric bodies. The isotropic eddy viscosity in this model is defined as

$$\nu_t = c_\mu \sqrt{k} l_\mu$$

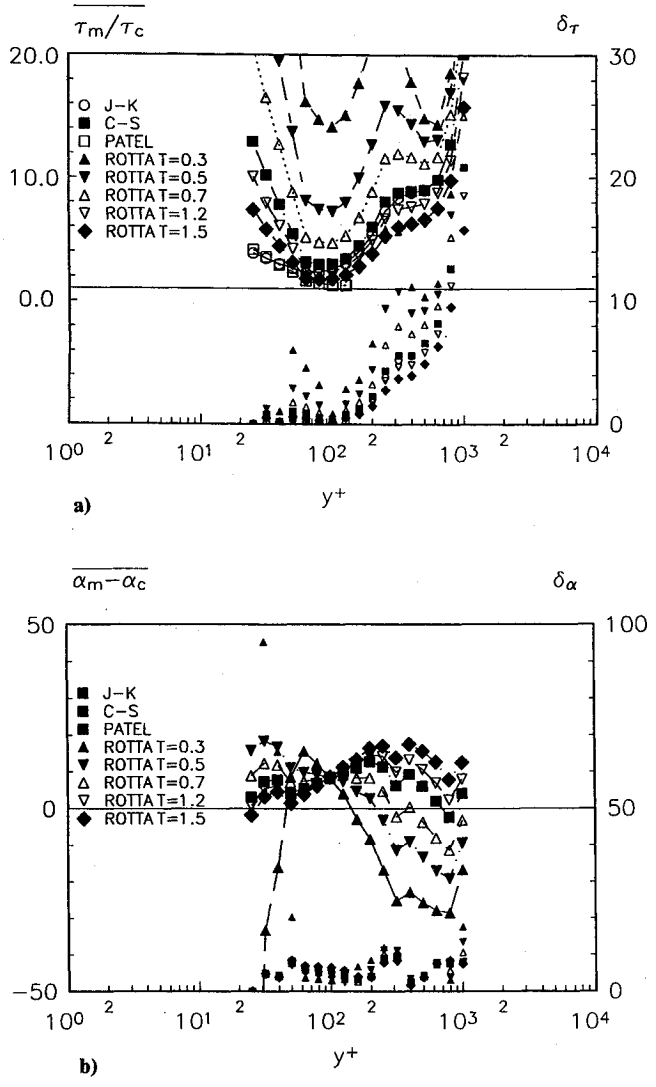

Fig. 6 a) Average magnitude ratio and b) average angle difference and the standard deviations on these quantities around the mean calculated with several models for Bissonnette-Mellor low *Re* flow. Right-hand-side ordinate and smaller symbols are used for the standard deviations.

$$l_\mu = c_l y[1 - \exp(-R_y/A_\mu)] \qquad c_l = \kappa c_\mu^{-3/4}$$

$$R_y = \sqrt{k}\,(y/\nu) = \text{turbulent Reynolds number}$$

$$A_\mu = 70 \qquad c_\mu = 0.09 \qquad \kappa = 0.418$$

$$k = \text{TKE} = \frac{\overline{u^2} + \overline{v^2} + \overline{w^2}}{2}$$

(k = TKE = turbulent kinetic energy) and the stresses in Cartesian coordinates could be computed using[44]

$$\overline{u_i u_j} = -2\nu_t S_{ij} + 2k\delta_{ij}/3$$

$$S_{ij} = \tfrac{1}{2}(U_{i,j} + U_{j,i})$$

$$\delta = 1 \quad \text{if} \quad i = j$$

$$= 0 \quad \text{if} \quad i \neq j$$

($\overline{u_i u_j}$ is the Reynolds-averaged kinematic stress tensor, $U_{i,j}$ is the partial derivative of U_i with respect to j, and $i = 1,2,3$; $j = 1,2,3$).

After neglecting the derivatives other than those with respect to y, the stresses in this study are computed using

$$-\overline{uv}_{FS} = \nu_t \frac{\partial U}{\partial y} \qquad -\overline{vw}_{FS} = \nu_t \frac{\partial W}{\partial y}$$

The validity of the equations for the turbulence model as given was defined to be restricted to the viscous sublayer, buffer layer, and a part of the fully turbulent layer. Therefore, the comparison with the data is only meaningful below $y^+ = 150$ (Ref. 45).

D. Johnson-King Model

The eddy viscosity model introduced by Johnson and King[46] (J-K) for two-dimensional flows subject to strong pressure gradients and separation was extended to three-dimensional flows by Abid.[47] Instead of using the wall skin friction as the Cebeci-Smith model does, the model utilizes the maximum shear stress in the layer (τ_M) to define the eddy viscosities and the Van Driest damping function, which is effective near the wall. The inner layer eddy viscosity, which has the same form as the Cebeci-Smith model, differs due to the use of the

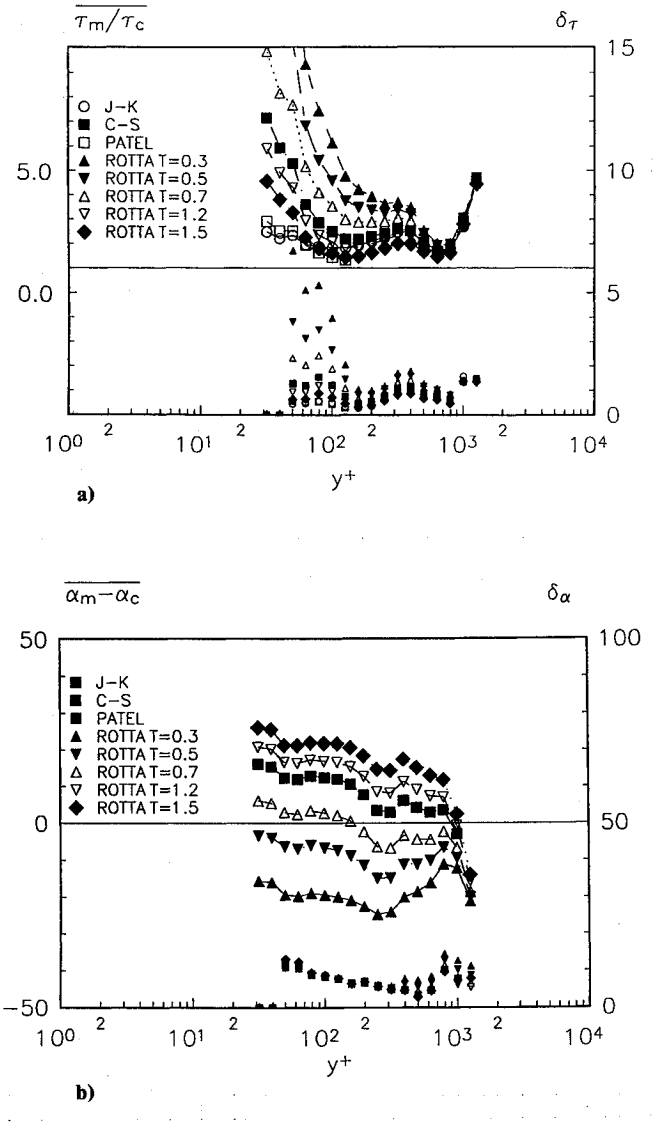

Fig. 7 a) Average magnitude ratio and b) average angle difference and the standard deviations on these quantities around the mean calculated with several models for Bissonnette-Mellor high *Re* flow. Right-hand-side ordinate and smaller symbols are used for the standard deviations.

maximum shear stress in the layer. The model is defined as follows:

$$\nu_{ti} = F^2 l\left(\frac{\tau_M}{\rho}\right)^{1/2}$$

$$F = 1 - \exp\left(-y\frac{(\tau_M/\rho)^{1/2}}{\nu A^+}\right) \qquad l = \kappa y$$

$$\frac{\tau_M}{\rho} = (\overline{uv}^2 + \overline{vw}^2)^{1/2}_{\max} \qquad A^+ = 15$$

The outer eddy viscosity was also modified to take into account the effect of the maximum shear stress in the outer layer. The outer layer eddy viscosity is defined as

$$\nu_{to} = \sigma(0.0168)\gamma_k \int_0^\infty (U_e - \sqrt{U^2 + W^2})\, dy$$

where σ parameter is found when the relation

$$\left(\frac{\tau_M}{\rho}\right) = \nu_t\left[\left(\frac{\partial U}{\partial y}\right)^2 + \left(\frac{\partial W}{\partial y}\right)^2\right]^{1/2}_{\max}$$

is satisfied at the location in the layer where the shear stress is maximum. Once σ is found, the shear stresses are found using

$$-\overline{uv}_{FS} = \nu_t \frac{\partial U}{\partial y} \qquad -\overline{vw}_{FS} = \nu_t \frac{\partial W}{\partial y}$$

where

$$\nu_t = \nu_{to}[1 - \exp(-\nu_{ti}/\nu_{to})]$$

The maximum shear stress magnitude is found by Johnson-King and Abid using an ordinary differential equation derived from the TKE equation, which is valid along a path where the shear stress is maximum. We do not evaluate the validity of this ordinary differential equation. Here, the experimental magnitude and y location of the maximum shear stress were used in evaluating other aspects of this model. The constant multiplier σ in the ν_{to} equation was found by Newton iteration and by using the experimental τ_M and mean flow gradients.

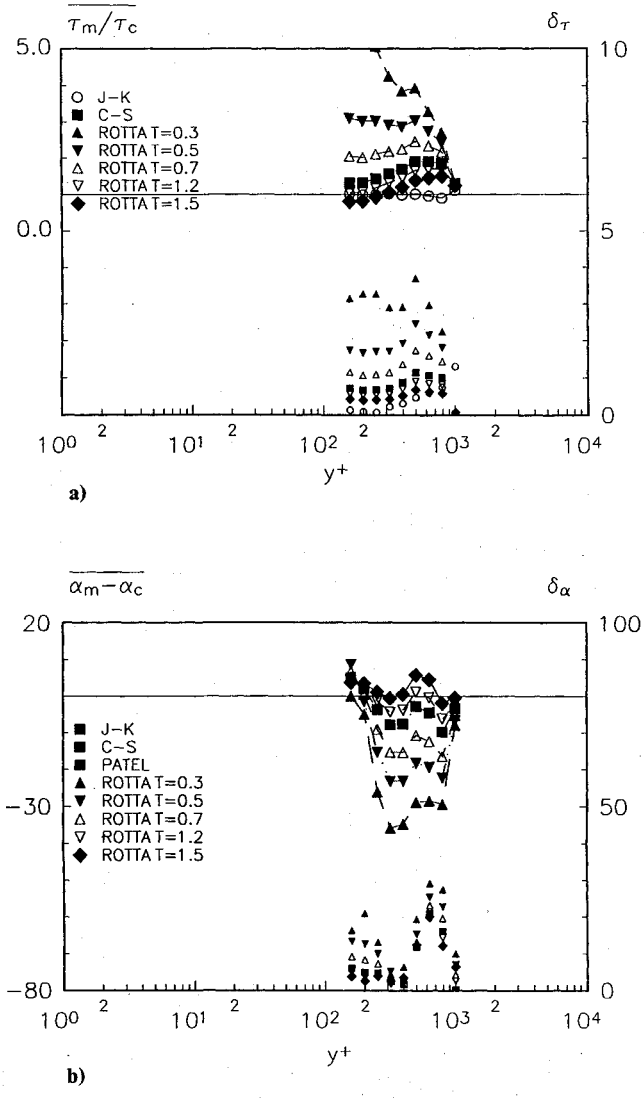

Fig. 8 a) Average magnitude ratio and b) average angle difference and the standard deviations on these quantities around the mean calculated with several models for Lohmann flow. Right-hand-side ordinate and smaller symbols are used for the standard deviations.

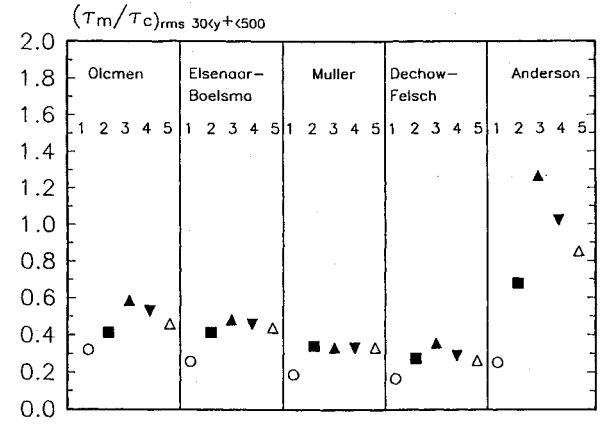

Fig. 9 Root mean square magnitude ratio calculated around 1.0 for pressure-driven flow data in the $30 < y^+ < 500$ range: 1 = J-K, 2 = C-S, 3 = Rotta $T = 0.3$, 4 = Rotta $T = 0.5$, 5 = Rotta $T = 0.7$ models.

IV. Results and Discussion

For all of the data sets the $\overline{\tau_m/\tau_c}$ and standard deviation of this quantity about the average and the average angle difference and the standard deviation of this quantity are plotted.

For the models that use a single eddy viscosity for both components of calculated shear stress (J-K, C-S, and Patel models), the angle difference can be derived to be

$$\alpha_m - \alpha_c = \arctan\left(\frac{-\overline{vw}}{-\overline{uv}}\right)_m - \arctan\left(\frac{\partial W/\partial y}{\partial U/\partial y}\right)_m$$

In this equation the right-hand side consists of only the derived quantities from the measured data, which shows that unless an anisotropic eddy viscosity is used in the formulation of the calculation of the shear stresses, no effect of the model exists on the angle difference. Therefore, only Rotta's model could affect or capture the angle difference. In Figs. 1-8, the plots of this quantity for the C-S, J-K, and Patel models are denoted with the same symbols. For the J-K, C-S, and Patel models the average angle difference shows the mean of the difference of measured shear stress vector direction and the mean velocity gradient vector directions.

In the near-wall range where Patel's model is valid, the Elsenaar-Boelsma and Lohmann flows had only four and three points, respectively. These points are not presented in the figures. For Dechow-Felsch, Anderson-Eaton, Ölçmen, and Müller flows, Patel's model calculates shear stress magnitudes more than the other models at most of the y^+ locations, which results in mean magnitude ratios within the range of 0.5 ~ 1.2. For the Bissonnette-Mellor data, Patel's model also

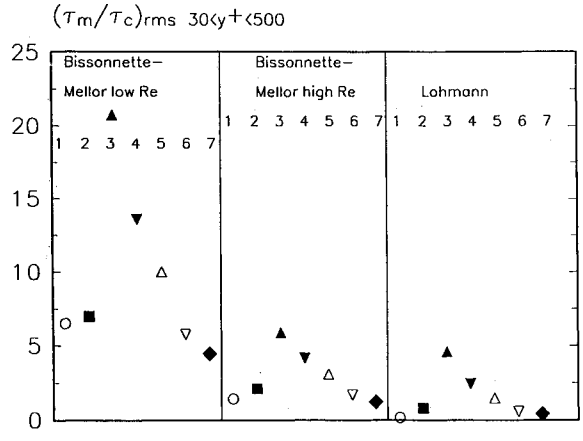

Fig. 10 Root mean square magnitude ratio calculated around 1.0 for shear-driven flow data in the $30<y^+<500$ range: 1 = J-K, 2 = C-S, 3 = Rotta $T = 0.3$, 4 = Rotta $T = 0.5$, 5 = Rotta $T = 0.7$, 6 = Rotta $T = 1.2$, 7 = Rotta $T = 1.5$ models.

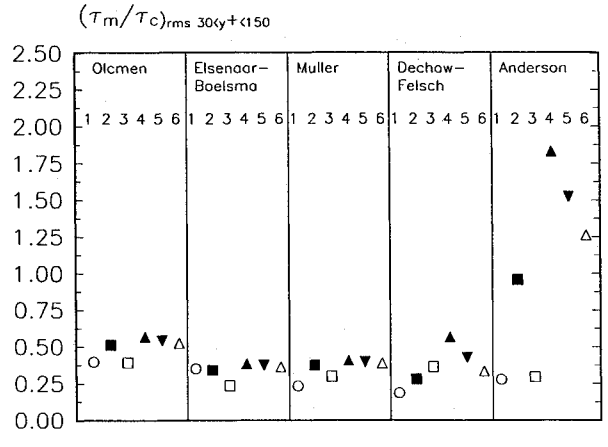

Fig. 11 Root mean square magnitude ratio calculated around 1.0 for pressure-driven flow data in the $30<y^+<150$ range: 1 = J-K, 2 = C-S, 3 = Patel, 4 = Rotta $T = 0.3$, 5 = Rotta $T = 0.5$, 6 = Rotta $T = 0.7$ models.

underestimates the shear stress magnitude just as the other models do, resulting in mean magnitude ratios larger than 1.

The C-S model for all of the data sets calculates the mean magnitude ratio to be larger than 1 for y^+ of the order of 100. Beginning at different y^+ locations, the calculated mean magnitude ratios for the pressure driven data are smaller than 1. For the Ölçmen flow the magnitude ratio is higher than 1 below $y^+ = 20$, decreases below 1 and is again higher than 1 with increasing y^+. For the shear-driven data the magnitude ratios are always large in the layers.

Like the C-S model, Rotta's model, even with varying values of the anisotropy constant, overcalculates the magnitude ratios near the wall for all data sets except for the Ölçmen flow. For this flow between $y^+ = 20$–60 the magnitude ratio is low. The proximity of the mean magnitude ratio to unity not only differs with the anisotropy constant but also with the data sets and with different regions in the profiles. Among the anisotropy constants tested for the Ölçmen and Elsenaar-Boelsma flows, $T = 0.7$ works best; for the Müller flow a value of $T = 0.3$ is needed. For Dechow-Felsch and Anderson flows $T = 0.7$ works best until $y^+ = 200$ and $y^+ = 150$, respectively; above these locations $T = 0.5$ gives better agreement for both flows. For the shear-driven flows, $T = 1.5$ works best.

Except for the Bissonnette-Mellor data sets $(\overline{\tau_m/\tau_c})$ values calculated using the J-K model mostly lie in the range of 0.5–1.4. For the Bissonnette-Mellor data sets, the average magnitude ratios are closer to 1 than any other model in the near-wall region below $y^+ = 60$. Like the other models, the magnitude ratios calculated with this model in the other regions are well above the value of 1. For Lohmann's data, the calculated shear stress magnitudes with the J-K model are in good agreement with the measured shear stresses. For the pressure-driven data, the J-K model estimates higher $(\overline{\tau_m/\tau_c})$ values than Patel's model and the values are closer to 1.

For different data sets and at different y^+ locations of the profiles, Rotta's model with different T anisotropy constants calculates average angle differences closer to zero. Whereas for the Elsenaar-Boelsma flow $T = 0.7$ is the best observed, Müller's flow needs values of the anisotropy constant greater than 1. For the Dechow-Felsch and Anderson data sets, $T = 0.3$ works best. However, for the Bissonnette-Mellor low Re data very near the wall, $T = 1.5$ works well, whereas above $y^+ = 100$, $T = 0.7$ predicts angle differences closer to zero. For the high Re data of Bissonnette-Mellor, $T = 0.7$ is seen to work well. For the Lohmann flow $T = 1.2$ and $T = 1.5$ work well at different y^+ locations. Thus the T constant, which results in closer values to 1 for $(\overline{\tau_m/\tau_c})$, does not necessarily work well in estimating the average angle difference.

In an attempt to find the best model in calculating the magnitude ratio and angle difference, the root mean square (rms) of the magnitude ratios around 1 and the rms of the angle differences around 0.0 were calculated using the following equations:

$$\left(\frac{\tau_m}{\tau_c}\right)_{\text{rms}} = \left\{\frac{1}{N}\sum_{i=1}^{N}\left[\left(\frac{\tau_m}{\tau_c}\right)_i - 1\right]^2\right\}^{1/2}$$

$$(\alpha_m - \alpha_c)_{\text{rms}} = \left[\frac{1}{N}\sum_{i=1}^{N}\left(\frac{\alpha_m}{\alpha_c}\right)_i^2\right]^{1/2}$$

The calculations were carried out twice for the $(\tau_m/\tau_c)_{\text{rms}}$: one between $30 < y^+ < 500$ and one between $30 < y^+ < 150$ locations in each profile of the data sets for each different model tested. Chosen y^+ locations correspond to the logarithmic region of the profiles of the data sets and to the near-wall region where Patel's model is valid. Therefore, only two values for the magnitude ratio and one value for the angle difference results for each model for each data set (Figs. 9–13). Since Patel's model does not have any effect on the rms angle difference, averaging was done only in the logarithmic region

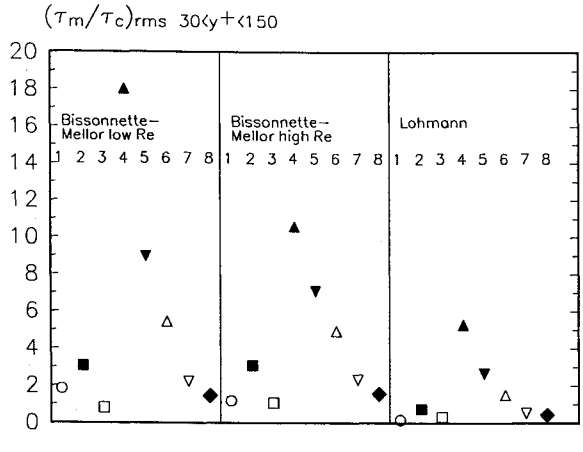

Fig. 12 Root mean square magnitude ratio calculated around 1.0 for shear-driven flow data in the $30<y^+<150$ range: 1 = J-K, 2 = C-S, 3 = Patel, 4 = Rotta $T = 0.3$, 5 = Rotta $T = 0.5$, 6 = Rotta $T = 0.7$, 7 = Rotta $T = 1.2$, 8 = Rotta $T = 1.5$ models.

to test Rotta's model. However Patel's model results are averaged only up to $y^+ = 150$.

Among the pressure-driven data sets, the J-K model is seen to work best in predicting the magnitude ratios for all of the flows for both regions. However, the location and magnitude of the maximum shear stress in the profiles in the original J-K model are found by solving the governing equations, whereas in the present study they are taken from the data.

Among the shear-driven data sets, Patel's model works best for the Bissonnette-Mellor data sets between $30 < y^+ < 150$; however, in the $30 < y^+ < 500$ region data are best described with Rotta's model with $T = 1.5$. For the Lohmann's flow, the J-K model performs best for both regions. The same conclusions were also observed from $[(\tau_m - \tau_c)/\tau_M]_{\text{rms}}$ (rms of the magnitude differences between measured and calculated shear stresses nondimensionalized with maximum shear stress at each station for each data set around zero) calculations, which are not presented here.

Both for pressure- and shear-driven data sets, different T constants in Rotta's model result in the least rms magnitude ratio. However, knowing a priori the one T constant that would work either for pressure-driven or shear-driven data sets proves to be difficult.

V. Conclusions

An evaluation of algebraic eddy viscosity models using eight different data sets and four different models was made. The average magnitude ratios calculated at different y^+ locations show that at different y^+ locations and for different data sets, different models perform better than the others. However, from the $(\tau_m/\tau_c)_{\text{rms}}$ calculated for each of the pressure-driven data sets for different models, the J-K model is seen to predict the magnitude ratio closer to unity than any other model for all of the flows, even for the region where Patel's model is valid. Among the shear-driven data sets, the Bissonnette-Mellor data is described best by Rotta's model with $T = 1.5$ whereas Lohmann's flow is best described by the J-K model. However, in the region up to $y^+ = 150$, both data sets of Bissonnette-Mellor are best described with Patel's model.

It was shown that models using an isotropic eddy viscosity term for the calculation of both components of shear stress (J-K, C-S, and Patel models) cannot affect the angle difference. It was also not possible to find one anisotropy constant for Rotta's model that could work for all of the data sets in the calculation of the angle differences. Also, an anisotropy constant that resulted in angle differences close to zero did not necessarily result in magnitude ratios closer to unity. For calculation of the angle differences, Rotta's model needed higher anisotropy constants for the Ölçmen and Müller flows. For the Elsenaar-Boelsma and Bissonnette-Mellor high Re data $T = 0.7$ is seen to perform best. However, for the Bissonnette-Mellor low Re data a value between 0.5 and 0.7 is best, and for the Lohmann flow a value between 1.2 and 1.5 is needed.

As one conclusion, the J-K model is recommended for the calculation of the shear stress magnitudes for the pressure-driven flows, provided that the magnitude and y location of the maximum shear stress are properly calculated by the ordinary differential equation in that model. With that restriction, that model calculates the magnitude ratios close to unity for all of the data sets. For the shear-driven data sets Patel's model or Rotta's model with anisotropy constants larger than 1 appear best of the examined models.

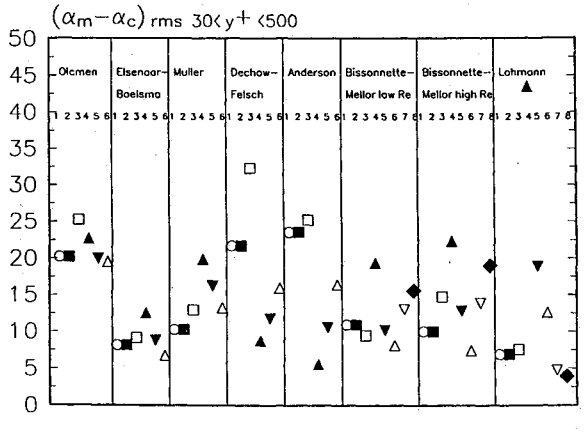

Fig. 13 Root mean square angle difference calculated around 0.0 for pressure- and shear-driven flow data: 1 = J-K, 2 = C-S, 3 = Patel, 4 = Rotta $T = 0.3$, 5 = Rotta $T = 0.5$, 6 = Rotta $T = 0.7$, 7 = Rotta $T = 1.2$, 8 = Rotta $T = 1.5$ models. Note results for Patel model only for $30 < y^+ < 150$.

Acknowledgments

The authors gratefully acknowledge the support of the Office of Naval Research, Edwin Rood and James A. Fein, Program Managers, and the Defense Advanced Research Projects Agency, Gary W. Jones, Program Manager.

References

[1]Rodi, W., "Examples of Turbulence Models for Incompressible Flows," *AIAA Journal,* Vol. 20, No. 7, 1982, pp. 872–879.

[2]Lakshminarayana, B., "Turbulence Modeling for Complex Shear Flows," *AIAA Journal,* Vol. 24, No. 12, 1986, pp. 1900–1917.

[3]Humphreys, D. A., and Lindhout, J. P. F., "Calculation Methods for Three-Dimensional Turbulent Boundary Layers," *Progress in Aerospace Sciences,* Vol. 25, No. 2, 1988, pp. 107–129.

[4]Launder, B. E., and Spalding, D. B., *Mathematical Models of Turbulence,* Academic Press, New York, 1972.

[5]Cebeci, T., and Smith, A. M. O., *Analysis of Turbulent Boundary Layers,* Academic Press, New York, 1974, Chap. 9.

[6]Bradshaw, P., Cebeci, T., and Whitelaw, J., *Engineering Calculation Methods for Turbulent Flow,* Academic Press, New York, 1981, Chaps. 3, 4.

[7]Rodi, W., *Turbulence Models and Their Application in Hydraulics,* International Association for Hydraulic Research, Delft, the Netherlands, 1980.

[8]Launder, B. E., Reece, G. J., and Rodi, W., "Progress in the Development of a Reynolds Stress Turbulence Closure," *Journal of Fluid Mechanics,* Vol. 68, Pt. 3, 1975, pp. 537–566.

[9]Tennekes, H., and Lumley, J. L., *A First Course in Turbulence,* MIT Press, Cambridge, MA, 1st printing 1972, 11th printing 1987, Chap. 2.

[10]Kline, S. J., Cantwell, B., and Lilley, G. M. (eds.), *Complex Turbulent Flows: Comparison of Computation and Experiment, Vol. II, Taxonomies, Reporters Summaries, Evaluation and Conclusions,* Stanford Univ. Press, Stanford, CA, 1982.

[11]Kline, S. J., Cantwell, B., and Lilley, G. M. (eds.), *Complex Turbulent Flows: Comparison of Computation and Experiment, Vol. III, Comparison of Computation with Experiment, and Computors' Summary Reports,* Stanford Univ. Press, Stanford, CA, 1982.

[12]Marvin, J. G., "Turbulence Modeling for Computational Aerodynamics," *AIAA Journal,* Vol. 21, No. 7, 1983, pp. 941–955.

[13]Wilcox, D. C., and Rubesin, M. W., "Progress in Turbulence Modeling for Complex Flowfields Including the Effect of Compressibility," NASA TP 1517, April 1980.

[14]Cebeci, T., Kaups, K., and Ramsey, J. A., "A General Method for Calculating Three-Dimensional Compressible Laminar and Turbulent Boundary Layers on Arbitrary Wings," NASA CR-2777, Jan. 1977.

[15]Baldwin, B. S., and Lomax, H., "Thin Layer Approximation and Algebraic Model for Separated Flows," AIAA Paper 78-257, Huntsville, AL, Jan. 1978.

[16]Visbal, M., and Knight, D., "The Baldwin-Lomax Turbulence Model for Two-Dimensional Shock-Wave/Boundary-Layer Interactions," *AIAA Journal,* Vol. 22, No. 7, 1984, pp. 921–928.

[17]Kirtley, K., and Lakshminarayana, B., "Computation of Internal Incompressible Separated Flows Using a Space Marching Technique," AIAA Paper 85-1624, Cincinnati, OH, July 1985.

[18]Sugavanam, A., "Evaluation of Low Reynolds Number Turbulence Models for Attached and Separated Flows," AIAA Paper 85-0375, Reno, NV, Jan. 1985.

[19]Horstman, C. C., and Hung, C. M., "Computation of Three-Dimensional Turbulent Separated Flow at Supersonic Speeds," *AIAA Journal,* Vol. 17, No. 11, 1979, pp. 1155, 1156.

[20]Kussoy, M. I., Horstman, C. C., and Viegas, J. R., "An Experimental and Numerical Investigation of a Three-Dimensional Shock Separated Turbulent Boundary Layer," *AIAA Journal,* Vol. 18, No. 12, 1980, pp. 1477–1484.

[21]Rotta, J. C., "A Family of Turbulence Models for Three-Dimensional Thin Shear Layers," *Turbulent Shear Flows 1,* edited by F. Durst et al., Springer-Verlag, Berlin, 1979, pp. 267–278.

[22]Rhyming, I. L., and Fannelop, T. K., "A Three-Dimensional Law-of-the-Wall Including Skewness and Roughness Effects," International Union of Theoretical and Applied Mechanics Symposium, Berlin, May 1982; also, Fernholz, H. H., and Krause, E. (eds.), *Three-Dimensional Turbulent Boundary Layers,* Springer-Verlag, Berlin, 1982, pp. 324–342.

[23]Humphreys, D. A., "Viscous Flow—Its Analysis and Computation," Aeronautical Research Inst. of Sweden Rept. 142, Stockholm, April 1986.

[24]Cousteix, J., "Integral Method and Turbulence Models Applied to Three-Dimensional Boundary Layers," International Union of Theoretical and Applied Mechanics Symposium, Berlin, May 1982; also, Fernholz, H. H., and Krause, E. (eds.), *Three-Dimensional Turbulent Boundary Layers,* Springer-Verlag, Berlin, May, 1982, pp. 286–297.

[25]Van Den Berg, B., Humphreys, D. A., Krause, E., and Lindhout, J. P. F., "Three-Dimensional Turbulent Boundary Layer Calculations and Experiments," *Notes on Numerical Fluid Mechanics, Volume 19,* Vieweg and Sohn Verlagsgesellschaft mbH, Braunschweig, Germany, 1988.

[26]Bradshaw, P., "Physics and Modelling of Three-Dimensional Boundary Layers," AGARD-Rept. 741, *Computation of Three-Dimensional Boundary Layers Including Separation,* Neuilly sur Seine, France, Feb. 1987, pp. 2–1, 2–19.

[27]Fernholz, H. H., and Vagt, J. D., "Turbulence Measurements in an Adverse-Pressure Gradient Three-Dimensional Turbulent Boundary Layer Along a Circular Cylinder," *Journal of Fluid Mechanics,* Vol. 111, Oct. 1981, pp. 233–269.

[28]Anderson, S. D., and Eaton, J. K., "An Experimental Investigation of Pressure-Driven Three-Dimensional Turbulent Boundary Layers," Thermosciences Div., Dept. of Mechanical Engineering, Stanford, Univ., Stanford, CA, June 1987.

[29]Van Den Berg, B., "Three-Dimensional Shear Layer Experiments and Their Use as Test Cases for Calculation Methods," AGARD-Rept. 741, *Computation of Three-Dimensional Boundary Layers Including Separation,* Neuilly sur Seine, France, 1987, pp. 3–1, 3–19.

[30]Anderson, S. D., and Eaton, J. K., "Experimental Study of a Pressure-Driven Three-Dimensional Turbulent Boundary Layer," *AIAA Journal,* Vol. 25, No 8, 1987, pp. 1086–1092.

[31]Dechow, R., and Felsch, K. O., "Measurements of the Mean Velocity and of the Reynolds Stress Tensor in a Three-Dimensional Turbulent Boundary Layer Induced by a Cylinder Standing on a Flat Wall," *Symposium on Turbulent Shear Flows,* The Pennsylvania State Univ., University Park, PA, April 1977, pp. 9.11–9.20.

[32]Dechow, R., "Mittlere Geschwindigkeit und Reynoldsscher Spannungstensor in der dreidimensionale turbulenten Wandgrenzschicht von einen Stehenden Zylinder," Mitteilungen des Instituts für Strömungsmechanik und Strömungsmoschinen, Universitat (TH) Karlsruhe, Germany, Vol. 21, March 1977.

[33]Müller, U. R., "Measurement of the Reynolds Stresses and the Mean Flow Field in a Three-Dimensional Pressure-Driven Boundary Layer," *Journal of Fluid Mechanics,* Vol. 119, June 1982, pp. 121–153.

[34]Elsenaar, A., and Boelsma, S. H., "Measurements of the Reynolds Stress Tensor in a Three-Dimensional Turbulent Boundary Layer Under Infinite Swept Wing Conditions," National Aerospace Lab., NLR TR 74095 U, The Netherlands, July 1974.

[35]Ölçmen, M. S., "An Experimental Study of a Three-Dimensional Pressure-Driven Turbulent Boundary Layer," Ph.D. Dissertation, Aerospace and Ocean Engineering Dept., Virginia Polytechnic Inst. and State Univ., Blacksburg, VA, 1990.

[36]Bissonnette, L. R., and Mellor, G. L., "Experiments on the Behavior of an Axisymmetric Turbulent Boundary Layer with a Sudden Circumferential Strain," *Journal of Fluid Mechanics,* Vol. 63, Pt. 2, 1974, pp. 369–413.

[37]Lohmann, R. P., "The Response of a Developed Turbulent Boundary Layer to Local Transverse Surface Motion," *Journal of Fluids Engineering,* Vol. 98, Series I, No. 3, 1976, pp. 354–363.

[38]Ailinger, K., " Measurements of Surface Shear Stresses under a Three-Dimensional Turbulent Boundary Layer using Oil-Film Laser Interferometry," M.S. Thesis, Aerospace and Ocean Engineering Dept., Virginia Polytechnic Inst. and State Univ., Blacksburg, VA, 1990.

[39]Schumann, U., "Realizability of Reynolds-Stress Turbulence Models," *Physics of Fluids,* Vol. 20, No 5, 1977, pp.721–725.

[40]Cebeci, T., "Problems and Opportunities with Three-Dimensional Boundary Layers," AGARD-Rept. 719, Neuilly sur Seine, France, 1984, pp. 6–1, 6–35.

[41]Rotta, J. C., "On the Effect of the Pressure Strain Correlations on the Three-Dimensional Turbulent Boundary Layers," *Turbulent Shear Flows 2,* edited by F. Durst et al., Springer-Verlag, Berlin, 1980, pp. 17–24.

[42]Wolfshtein, M., "The Velocity and Temperature Distribution in One-Dimensional Flow with Turbulence Augmentation and Pressure Gradient," *International Journal of Heat and Mass Transfer,* Vol. 12, No. 3, 1969, pp. 301–318.

[43]Chen, H. C., and Patel, V. C., "Near-Wall Turbulence Models for Complex Flows Including Separation," *AIAA Journal,* Vol. 26, No. 6, 1988, pp. 641-648.

[44]Stern, F., Yoo, S. Y., Patel, V. C., "Interactive and Large-Domain Solutions of Higher-Order Viscous-Flow Equations," *AIAA Journal,* Vol. 26, No. 9, 1988, pp. 1052-1060.

[45]Patel, V. C., and Chen, H. C., "Turbulent Wake of a Flat Plate," *AIAA Journal,* Vol. 25, No. 8, 1987, pp. 1078-1085.

[46]Johnson, D. A., and King, L. S., "A New Turbulence Closure Model for Boundary Layer Flows with Strong Adverse Pressure Gradients and Separation," *AIAA Journal,* Vol. 23, No. 11, 1985, pp. 1684-1692.

[47]Abid, R., "Extension of the Johnson-King Turbulence Model to Three-Dimensional Flows," AIAA 26th Aerospace Sciences Meeting, AIAA Paper 88-0223, Reno, NV, Jan. 1988.